Phase behaviors of supercooled water: Reconciling a critical point of amorphous ices with spinodal instability

Hideki Tanaka
Department of Polymer Chemistry, Graduate School of Engineering, Kyoto University, Sakyo, Kyoto 606-01, Japan

(Received 20 May 1996; accepted 17 June 1996)

The anomalies of supercooled water in thermodynamic response functions at atmospheric pressure, the phase transition between low and high density amorphous ices (LDA and HDA), and a predicted fragile–strong transition are accounted for in a unified manner by reconciling an idea due to Stanley and co-workers introducing a second critical point separating LDA and HDA ices with a conjecture proposed by Speedy that LDA is a different phase from a normal water, called water II. The reconciliation is made on the basis of results from extensive molecular dynamics simulations at constant pressure and temperature. It is found that there exist large gaps around temperature 213 K in thermodynamic, structural, and dynamic properties at atmospheric pressure, suggesting liquid–liquid phase transition. This transition is identified with an extension of the experimentally observed LDA–HDA transition in high pressure to atmospheric pressure. Thus, we propose a new phase diagram where the locus of the second critical point is moved into negative pressure region. With this simple modification, it becomes possible to account for the divergence of the thermodynamic response functions at atmospheric pressure in terms of the critical point and the spinodal-like instability of HDA. The unstable HDA undergoes a transition to LDA phase in lower temperature. The transition is also observed in high pressure region such as 200 MPa while it disappears at negative pressure, -200 MPa. This reinforces our proposed phase diagram in which there is no continuous path from a supercooled state to LDA at atmospheric pressure. It is argued that the HDA–LDA transition is accompanied by a fragile–strong transition. A possible mechanism of avoiding crystallization of aqueous solutions is also discussed in terms of a difference in hydrogen bond number distribution between LDA and HDA. © *1996 American Institute of Physics.* [S0021-9606(96)00436-9]

I. INTRODUCTION

Water exhibits various anomalies in thermodynamic response functions such as heat capacity and isothermal compressibility.[1–3] It has been shown experimentally that at least two metastable phases of amorphous ices exist[4] together with a rich variety of solid phases;[5] they are referred to as low density amorphous ice (LDA) and high density amorphous ice (HDA). The transition between LDA and HDA is first order because it exhibits a hysteresis in pressure-induced transformation.[6] In an intermediate (supercooled) state to connect water above the melting temperature T_m with LDA phase, those thermodynamic properties together with several transport properties tend to diverge with a power low behavior when approaching to T_s, 228 K.[7,8] These anomalies were accounted for by many authors with various ideas and conjectures. Among them, the most notable one was due to Speedy, which is called ''stability-limit conjecture.''[9] He explained the divergence of thermodynamic properties in supercooled state in conjunction with the liquid–vapor spinodal. The liquid spinodal line is the limit of mechanical stability of the liquid state with respect to fluctuations toward a thermodynamically stable phase. The liquid spinodal line begins at the liquid–gas critical point. In temperature–pressure ($p-T$) plane, this line decreases monotonically with decreasing temperature along a path lying below the liquid–gas coexistence curve in positive pressure region and goes into negative pressure. The liquid spinodal line has a minimum at negative pressure and passes back to positive pressure as the temperature decreases further. The increasingly anomalous thermodynamic behavior of liquid water in the low temperature region can be interpreted via such a reentrant spinodal line, which divides the metastable supercooled water from stable ice. Stanley and Teixeira[10] accounted for the anomalies at 228 K from a different view point, called ''percolation model'' in which emphasis was placed on the fact that fully hydrogen bonded water molecules are not randomly distributed but rather correlated. The origin of the instability of supercooled water is, in either account, an increasing fluctuation of a long ranged tetrahedral connectivity of water molecules. This idea which seems to be intuitive but persuasive was further extended by Sasai[2,11] and by Sastry *et al.*[12] with a mean field approximation.

The conjectured minimum in liquid spinodal line, at which the temperature of maximum density line terminates,[13] has not been directly observed due to the experimental difficulties. Poole *et al.*[14] carried out molecular dynamics (MD) simulations over a wide range of stable, metastable, and unstable liquid-state points, and demonstrated that liquid spinodal line decreases monotonically with decreasing temperature and does not reenter into the positive pressure region. They concluded that the anomalies are related to a second

critical point from which a LDA–HDA phase boundary appears. According to their estimation, the second critical point was located at around 200 MPa. The phase diagram they proposed suggests that if crystallization does not intervene, supercooled water is further cooled without a phase transition to LDA which has a glass transition temperature at T_g, 136 K.[15–18] It is, however, not clear how to reconcile the critical behaviors with the fact that water loses its anomalies[5] around the same pressure range as the critical point was located by them[14] and what happens to the thermodynamic response functions when approaching to the critical point.

It has long been argued whether supercooled water has a thermodynamically continuous path to LDA.[19–25] Recently, Speedy proposed the other conjecture that LDA (LDA becomes liquid above T_g, called water II) has no continuous path from normal water at atmospheric pressure.[26] It is appropriate here to note, that we specify LDA and HDA for terms which are distinct phases from each other having fairly different densities, potential energies, etc., but they may be either liquid and amorphous phase; use of LDA and HDA is conventional and both phases are liquid above the corresponding glass transition temperature. An entropy difference between ice and LDA must be very small in order for the free energy surfaces of LDA and supercooled water to touch in a narrow range between 228 K (T_s, the conjectured stability limit) and 233 K (T_2, the homogeneous nucleation temperature, the limit of experimental supercooling). The estimation of the entropy was made based on the measured thermodynamic properties and the model for calculation of the configurational entropy of LDA. It was shown within the framework of the model adopted that LDA is neither the same phase as supercooled water nor is created from supercooled water via first order transition. This is in sharp contrast to MD simulation study.[14] The phase diagram for these amorphous ices including supercooled liquid state is still controversial.

In order to model the phase behavior of liquid water, Poole *et al.*[27] developed a van der Waals type equation. In their model, the free energy is divided into two parts; the van der Waals free energy and the free energy due to hydrogen bonds, both of which are functions of the volume and have minima at fairly different molar volumes. Their model predicts, though qualitatively, anomalous thermodynamic properties of water, such as density maximum temperature, the divergence in the compressibility and the heat capacity with assignment of appropriate parameters. At sufficiently low temperature, the free energy in this model has two minima. They associated the LDA↔HDA transition with the transition from a free energy local minimum to another in density coordinate axis. However, this model also yields a different phase diagram by a slight change of the parameters: It was demonstrated that though two phase diagrams are apparently so different, an introduction of two minima of the free energy against volume results in two different phase diagrams with changing the hydrogen bond energy. Although this model calculation contributes significantly to our understanding of the origin of the anomalies of supercooled water, the problem posed as to the thermodynamic continuity of supercooled water is not resolved by this model.

We have performed long MD simulations at constant pressure in order to reexamine phase behaviors and found discontinuities in thermodynamic and structural properties around 213 K.[28] This finding enables us to reconcile both ideas proposed by Poole *et al.*[14] and by Speedy.[26] Thus, a phase diagram becomes simpler and comprehensible. The free energies of LDA and HDA are analyzed by dividing them into several contributions, the potential energies at local minimum structures, harmonic and anharmonic vibrational free energies, and the configurational entropies. The configurational entropies of LDA and HDA are calculated from the remaining components, assuming first-order phase transition between LDA and HDA. Moreover, we show that the observed large differences in thermodynamic properties between two phases entails a predicted fragile–strong transition[29] in pure water. Analysis of hydrogen bond number per molecule makes a difference between LDA and HDA clearer and we deduce a possible mechanism for avoiding crystallization in aqueous solutions of salt, alcohol, and hydrogen peroxide. Those investigations also serve to understanding roles of water in biological system such as cryopreservation and solar system, particularly in comets.

The present paper is organized as follows. The method of MD simulations is briefly described in Sec. II. Results obtained from MD simulations are presented and a new phase diagram is proposed in Sec. III. Our findings on phase diagram for supercooled water are concluded with a few remarks in Sec. IV.

II. MOLECULAR DYNAMIC SIMULATIONS

MD simulations are performed with a fixed pressure of 0.1 MPa at several temperatures using Nosé–Andersen's constant temperature-pressure method.[30,31] The temperatures, T are set to 298, 273, 255, 233, 213, and 193 K. As an intermolecular interaction, TIP4P potential[32] is adopted. Its accuracy in reproducing thermodynamic properties at lower temperature was examined in detail by Poole *et al.*[33] The simulation time is ranging from 1 ns (298 K) to 20 ns (213 to 193 K), which is significantly longer than previous simulations. Those longer runs together with a different ensemble (NPT) can predict a different location of the critical point, which in turn leads to a different phase diagram. The number of molecules N is set to 216. Preliminary simulations with larger number of molecules (1728) do not change our conclusion given below. Because of slow equilibration in lower temperatures, the last configuration at 233 K is used for the initial configuration at 213 K, and so forth at 193 K. We select 500 to 5000 configurations each separated by 25 (at higher temperatures) to 2000 (at lower temperatures) time steps, with a step size of 5×10^{-16} s. Those configurations obtained from MD simulation are called instantaneous (I-) structures, from which various properties to be compared directly to experiment such as thermodynamic response functions, structure factors, transport coefficients, and spectral densities are calculated. The potential energy for those I-structures are composed of two contributions, (1) the poten-

tial energy of the minimum structures, and (2) upward shifts from (1) due to thermal energy. The minimum energy structures correspond to stable points in configuration space, and therefore, are free from thermal excitation. Those are called inherent[34] or quenched (Q-) structures.[2,3,35] The steepest descent minimization is applied to obtain Q-structures from I-structures generated by MD simulation.

Other MD simulations have also been performed at high (+200 MPa) and at low (−200 MPa) pressure in order to confirm our phase diagram proposed on the basis of MD simulation results at atmospheric pressure. The temperatures examined are limited to 253, 233, 213, and 193 (−200 MPa) and 233, 213, 193, and 173 K (+200 MPa). In MD simulation at high temperature and low pressure (298 and probably 273 K, −200 MPa), a cavitation occurs since there is an intersection with the liquid-spinodal line above (in temperature) which liquid state is mechanically unstable. Low mobility of water molecules in low temperature and at low pressure prevents us from obtaining reliable results, and therefore, the lowest temperature in the present simulation is limited to 193 K.

III. RESULTS AND DISCUSSION

A. Thermodynamic properties

In Fig. 1, plotted are the potential energies at 0.1 MPa (triangles) each averaged over a block composed of equally spaced 500 configurations of both I-structure and Q-structure as mentioned in the previous section. In order to remove a trivial temperature dependence from the calculated potential energy of I-structures, plotted are the potential energies subtracted by the harmonic part of the potential; $3RT$ where R is the gas constant. More interesting are the large differences in potential energies of both I- and Q-structures between 233 and 213 K. (The minimum energy value among 10 blocks at 213 K is plotted to avoid mixing of lower and higher energy states due to a large fluctuation; the chosen block belongs to the lower energy state, which continues for longer than 0.5 ns.) This suggests that, although liquid water at room temperature has a continuous path to a supercooled state down to 233 K, it undergoes a transition around 213 K to another state, whose energy is substantially (1.5 kJ mol^{-1}) lower than that at 233 K in Q-structure. The potential energy in Q-structure at 193 K is almost the same as the potential energy in Q-structure at 213 K. It should be noted, that this lower energy phase below 213 K has the potential energy higher by 1 kJ mol^{-1} than that of proton-disordered cubic ice; the mean potential energy over 100 Q-structures of proton disordered cubic ice with TIP4P model is −55.9 kJ mol^{-1}. If this lower energy phase is identified with LDA, the energy difference in our calculation is consistent with the measured heat release,[22] 1.3 kJ mol^{-1} at 150 K. A part of the measured heat release should be attributed to larger anharmonic energy of LDA than cubic ice.

In order to draw a phase diagram for supercooled water, a number of simulations at different pressures are required. It is not our scope to present a quantitative phase diagram but to examine the locus of the second critical point and to determine whether there is a continuous path from supercooled water to LDA at atmospheric pressure. Thus, we have carried out further MD simulations at high (+200 MPa) and low (−200 MPa) pressure. The potential energies for I-structure and Q-structure are shown in Fig. 1 (the trivial term, $3RT$ is subtracted in I-structure). An abrupt change in potential energy at +200 MPa is found between 193 and 173 K. The difference is somewhat smaller compared with that at 0.1 MPa. On the other hand, the potential energy at −200 MPa changes almost linearly with temperature, suggesting no transition occurs in the temperature range examined here. A similar plot for the density is given in Fig. 2. An abrupt change is also found in density at +200 MPa while no appreciable temperature dependence is seen in the systems under tensile pressure, −200 MPa. Therefore, the conclusion derived from the results at 0.1 MPa gains firm ground.

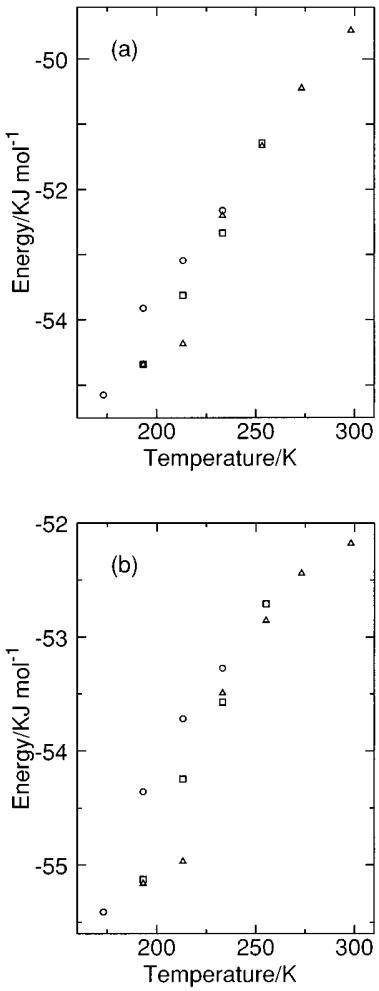

FIG. 1. Potential energy of instantaneous (a) and quenched (b) structures at various temperatures. Harmonic energy, $3RT$ is subtracted from the potential energy for Instantaneous structure. Individual points are the potential energies in kJ mol^{-1} averaged over 500 configurations. Triangle; pressure $p = 0.1$ MPa, circle; $p = +200$ MPa, square; $p = -200$ MPa. At pressure $p = 0.1$ MPa, the minimum energy value among 10 blocks at 213 K is plotted to avoid mixing of lower and higher energy states due to a large fluctuation (see text); the chosen block belongs to the lower energy state, which continues for longer than 0.5 ns.

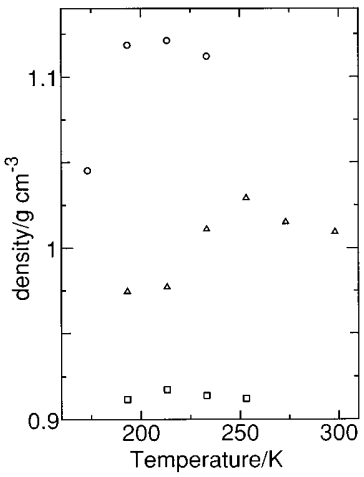

FIG. 2. Densities at various temperatures in g cm $^{-3}$ averaged over 500 configurations. Triangle; pressure $p = 0.1$ MPa, circle; $p = +200$ MPa, square; $p = -200$ MPa. At pressure $p = 0.1$ MPa and temperature 213 K, the mean density for the same block as in Fig. 1 is plotted.

As shown in Fig. 2, the gap in density is larger at high pressure than at atmospheric pressure although the reverse holds for potential energy. When we consider usual phase behaviors such as in liquid–gas equilibrium, the most appropriate order parameter to characterize behaviors in the vicinity of the critical point is a density difference between two phases. In the present simulation, the density of the system is allowed to fluctuate around a mean value. Hence, we calculate the density distributions which are shown in Fig. 3. At pressure $p = 0.1$ MPa, the distribution for the same block as in Fig. 1 (the lowest potential energy block) is shown. Clearly, each has a unimodal distribution. At high and atmospheric pressures, the center of distribution jumps from the high to low density with decreasing temperature while the center do not drift with decreasing temperature at -200 MPa. The order parameter is larger at higher pressure compared to that at atmospheric pressure. This suggests that the order parameter can be a vanishing value in certain low pressure. This is indeed the case of what we observe at -200 MPa. The coexistence line should be terminated at the second critical point which is located at a negative pressure higher than -200 MPa.[36]

It is not clear whether the large volume and energy changes at around 213 K are associated with a first-order phase transition from this limited size of simulations: The small system size blurs the distinction between first order phase (reversible) transition and (irreversible) spinodal instability. However, there must exist a critical point at around 213 K and at pressure lower than the atmospheric pressure. This is because a large density fluctuation, 0.03 g cm^{-3}, at 213 K compared with 0.01 g cm^{-3} at 233 K is attributed to vacillation between two distinct phases near the critical point. This situation is the same as a density of a finite system size in isothermal–isobaric condition near a gas–liquid critical point; the density fluctuates between gas and liquid phases.[40] In accordance with the large density fluctuation, the

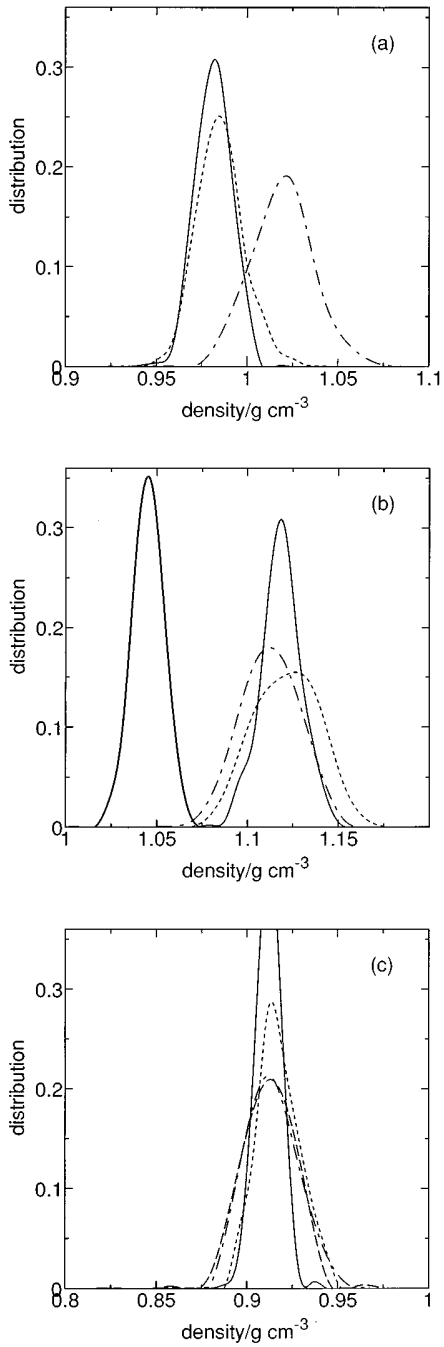

FIG. 3. Density distributions averaged over 500 configurations at various temperatures. (a) pressure $p = 0.1$ MPa, $T = 193$ K (solid line), $T = 213$ K (dotted line), $T = 233$ K (dash–dot line). (b) $p = +200$ MPa, $T = 173$ K (heavy solid line), $T = 193$ K (solid line), $T = 213$ K (dotted line), $T = 233$ K (dash–dot line). (c) $p = -200$ MPa, $T = 193$ K (solid line), $T = 213$ K (dotted line), $T = 233$ K (dash–dot line), $T = 253$ K (dashed line). At pressure $p = 0.1$ MPa and temperature 213 K, the distribution for the same block as in Fig. 1 is shown.

energy difference between the maximum and minimum energies at 213 K among the blocks (each composed of 500 configurations) amounts to 0.5 kJ mol^{-1}, which is much larger than 0.1kJ mol^{-1} at 233 K or 0.05 kJ mol^{-1} at 193 K.

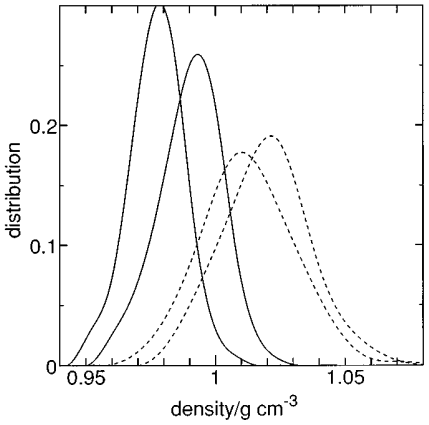

FIG. 4. Density distributions averaged over 500 configurations at $p = 0.1$ MPa and $T = 213$ K (solid lines) and $T = 233$ K (dotted lines). Two distributions at the same temperature are those averaged within the blocks which give maximum and minimum potential energies.

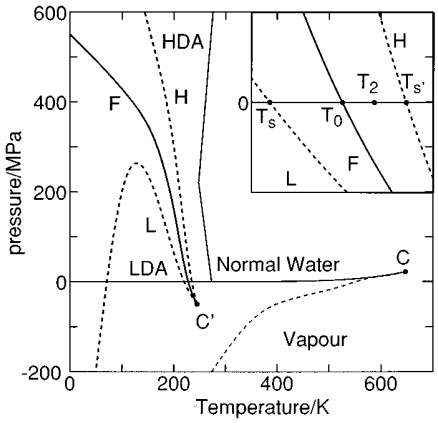

FIG. 5. Schematic phase diagram for water. Thin solid lines are coexistence lines of stable phases which separate liquid water from vapor and ice from liquid water. Thin dashed line is liquid spinodal. Boundaries of metastable states are shown by heavy solid line (F) for the coexistence line and by heavy dashed lines (L and H) for LDA spinodal above which LDA becomes unstable and for HDA spinodal below which HDA becomes unstable. The gas–liquid critical point is shown by C. The second critical point is denoted by C'.

The existence of the critical point is also suggested by the pressure dependence of the order parameter.

Since the second critical point is estimated to be close to 0.1 MPa and at 213 K, the thermodynamic properties are heavily influenced by the critical point. If the system size is limited, a transition between two phases occurs easily as mentioned above. The density distributions, which have the highest and lowest density (also having the highest and lowest energy) among 10 blocks at 213 K, are plotted in Fig. 4. The distribution for the lowest density block (its center is 0.977 g cm^{-3}) is almost the same as that at 193 K (0.974 g cm^{-3}) while the distribution for the highest density block has a center at 0.991 g cm^{-3} which is similar to the extrapolated density, 0.992 g cm^{-3} from those at 233 and 253 K. The system at 213 K indeed undergoes a facile transition between two phases. From those results, it is difficult to discriminate the spinodal instability from the phase transition near the critical point such as atmospheric pressure. However, water at 193 K is a different phase from water at 233 K. The divergent characters can be ascribed to the existence of the critical point and/or to the spinodal line since the spinodal line locates near the critical point. At high pressure, it is expected that the spinodal instability becomes important.

It is reasonable to consider that the phase boundary line continuously increases up to, say 400 MPa where LDA–HDA transition is experimentally observed.[6] Therefore, the transition at atmospheric pressure is induced by the same mechanism as the LDA–HDA phase transition observed experimentally.[4] This means that metastable supercooled water can be recast in the framework of LDA and HDA phases and that the divergent characters can also be related to the influences of the critical point and the spinodal instability.

B. Phase diagram for supercooled water

We propose a new phase diagram of metastable water as drawn in Fig. 5, which is, at a glance, similar to the picture of Stanley *et al.*[14,37] and others.[38,39] The spinodal line, the limit of stability of HDA, emerges from this critical point. As the temperature decreases, the HDA→LDA spinodal line first increases, reaching a maximum pressure point, and then goes down to the negative pressure again. Other spinodal and coexistence lines presumably increase monotonically. A transition from HDA to LDA at low temperature such as 77 K is unlikely to occur as was suggested by theoretical calculation[27] as well as experiments.[4,6]

A main difference from the previous study[14,37] is a locus of the second critical point, which is located in negative pressure region. At atmospheric pressure, HDA turns to LDA phase when the temperature goes down to the intersect with the HDA→LDA spinodal line. This is consistent with our observation that a substantial decrease in density is accompanied by HDA→LDA transition as shown in Fig. 2. Thus, all the divergences in supercooled water are ascribed to the spinodal instability at the temperature below which HDA becomes unstable and to the existence of the second critical point. It is reasonable that normal water, designated by Speedy,[26] is identified with water at temperature above the phase boundary, T_0. In our phase diagram, LDA (water II) is a different phase from water in supercooled state so that large fluctuations associated with the critical point are not observed in very high pressure region, which is consistent with the fact that water ceases to exhibit singular behaviors above 300 MPa.[5]

As water is cooled, it encounters the LDA→HDA spinodal line at $T_{s'}$ and the coexistence line at T_0. No transition occurs in our simulations until it reaches to the HDA→LDA spinodal line at T_s. However, crystallization to ice at T_2 prevents us from observing the transition. We can observe only the symptom of the spinodal instability in thermodynamic response functions. When heated, LDA should be transformed to HDA (normal water) after crossing $T_{s'}$. This transition is again not observed experimentally because LDA becomes ice at $T_1 (\simeq 150$ K). It is well known that, although

pressure is correctly reproduced by the use of TIP4P potential, the temperature obtained with this potential should shift upward by 10 to 20 K in order to compare with experiment.[14] That the divergences occur experimentally at 228 K is thus, in good correspondence to the discontinuity at about 213 K in our MD simulation.

C. Structural difference associated with the transition

It is essential to show water below 213 K is neither ice nor is partially crystalline form. Radial distribution functions (RDFs) and structure factors serve to discern a disordered form from crystalline. The structure factor

$$S(k)=\frac{1}{N}\left[\left(\sum_i \cos \mathbf{k}\cdot\mathbf{r}_i\right)^2+\left(\sum_i \sin \mathbf{k}\cdot\mathbf{r}_i\right)^2\right] \tag{1}$$

is also calculated from 500 configurations of I-structures for water and also 250 configurations of I-structure for cubic ice. Here, $\mathbf{k}$ is a wave vector, $k=|\mathbf{k}|$, and $\mathbf{r}_i$ stands for the position of the oxygen atom of ith water molecule. Five different proton disordered structures generated are used as initial configurations for MD simulations of ice at 213 K and 50 configurations from each simulation are sampled. Other conditions are the same as those for liquid state. The structure factors for liquid water at 193, 213, and 233 K are shown in Fig. 6 together with that for ice at 213 K. As shown in Fig. 6(a), cubic ice has sharp peaks characteristic of solid phase. On the other hand, that of water at 193 K is similar to that at 213 K having halo diffraction pattern, typical of liquid, or amorphous state. No pronounced peak appears in low wave number region and we need not worry about a partial crystallization. LDA thus obtained seems to be a different phase from crystalline structure. It is, however, noted that the system size fixes the lower limit on the wave vectors that can be studied and that the above result in very small wave vector range (specifically $k=0$) becomes incompatible with the large density fluctuation expected.

The RDFs for Q-structure are given in Fig. 7. Judging from the peak heights, the structure at 213 K is quite different from that of ice. As lowering the temperature from 298 K down to 233 K, only small difference is seen in RDF. The RDF at 213 K is clearly different from that 233 K, in particular the separation of the second peak from the first one is more distinct. On the other hand, a difference in RDF between 213 and 193 K is negligibly small in Q-structure, which implies that the system at 213 K sampled here is similar phase to that at 193 K and structural change below 213 K is quite small. The arrangement of molecules at 173 K and $+200$ MPa is similar to that at 193 K and 0.1 MPa while the RDF above 193 K is similar to that at 233 K and 0.1 MPa. The RDFs at negative pressure, -200 MPa are all similar to that at 193 K and 0.1 MPa (RDFs at ± 200 MPa are not shown here).

In Fig. 8, the distributions of pair interaction energy for Q-structures are depicted. Only pairs of water molecules separating less than 3.5 Å are taken into consideration. In cubic ice, there are two kinds of hydrogen bonds depending on rotation of the dihedral angle (around the axis parallel to the hydrogen bond) as seen in Fig. 8(a). In LDA at 193 K, the peak becomes broader and distinction between two kinds of hydrogen bonds becomes difficult. It is clear, from a comparison between those at 298 and 233 K [Fig. 8(b)], that a fairly large number of pairs are only loosely or not hydrogen bonded (the energy higher than -10 kJ mol^{-1}) and that the decrease in temperature reduces the number of high energy (i.e., defect) pairs while the distribution of strongly hydrogen bonded (stable) pairs remains almost unchanged. A further decrease of temperature by only 20 K, however, changes the distribution drastically. Most of defects suddenly disappear resulting in formation of stable hydrogen bonds. Although water below 213 K does not have a periodic molecular arrangement, local structure and tetrahedral connectivity are almost perfect. The distribution at 193 K overlaps almost completely with that at 213 K.

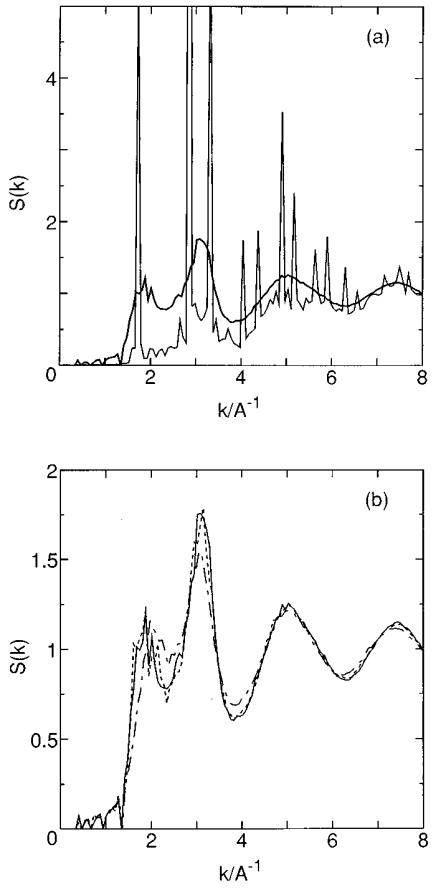

FIG. 6. Structure factors for oxygen–oxygen of water at 233, 213, and 193 K and at 0.1 MPa together with that for cubic ice at 213 K. (a) Water at 193 K (heavy solid line), cubic ice at 213 K (solid line), (b) water at 193 K (solid line), water at 213 K (dotted line), water at 233 K (dash–dot line).

D. Collective motions near potential well

We compare the density of state for intermolecular vibrational motions by performing a normal mode analysis. The densities of state for intermolecular vibrational motions calculated from Q-structures are given in Fig. 9(a). Difference between those at 298 and 233 K is insignificant whereas

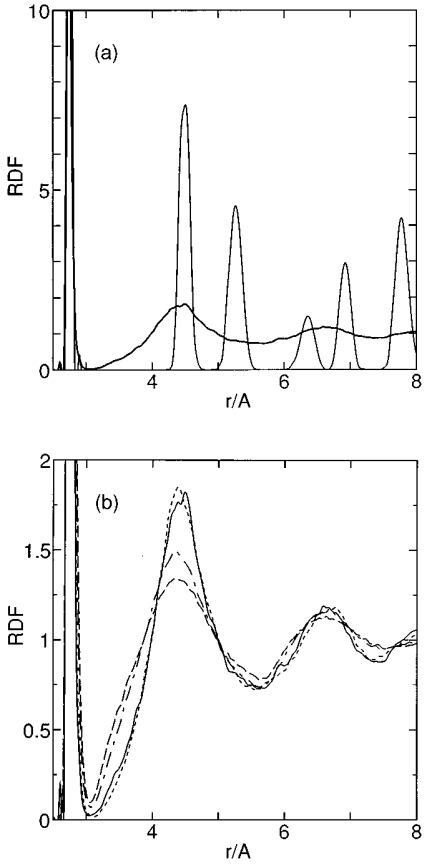

FIG. 7. Oxygen–oxygen radial distribution functions for water at 233, 213, and 193 K and at 0.1 MPa together with that for cubic ice at 213 K. (a) water at 193 K (heavy solid line), cubic ice (solid line). (b) water at 193 K (solid line), water at 213 K (dotted line), water at 233 K (dash–dot line), water at 298 K (dashed line).

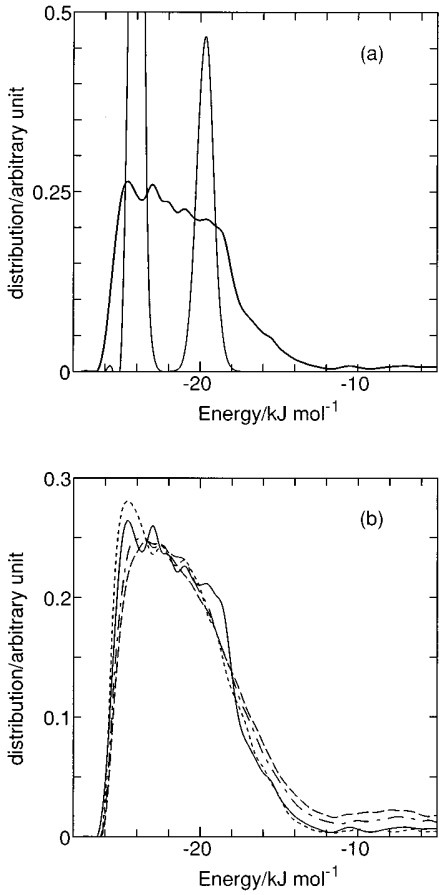

FIG. 8. Distributions of pair interaction energy for quenched structures at 233, 213, and 193 K and at 0.1 MPa together with that for cubic ice at 213 K. (a) water at 193 K (heavy solid line), cubic ice (solid line), (b) water at 193 K (solid line), water at 213 K (dotted line), water at 233 K (dash–dot line), water at 298 K (dashed line). The distributions are calculated for pairs of water molecules whose distances are smaller than 3.5 Å. The ordinate axis unit is arbitrary.

difference is large between those at 233 and 213 K. Lowering the temperature by only 20 K reduces number of modes between 300 and 500 cm^{-1}, which are mixed modes composed of translations and rotations of individual molecules and lead to a neighboring Q-structure with small excitation energy.[41] The densities of states for intermolecular vibrational motions are used for evaluation of harmonic free energies.

The densities of state for I-structures are given in Fig. 9(b). In the case of I-structures, there exist some imaginary frequency modes. The density of imaginary modes is plotted in negative frequency region of the figure. The number of imaginary modes is approximately 146.3 out of 1293 total modes (11.3%) at 298 K. The number is reduced remarkably and is approximately 83.7 (6.4%) at 233 K. The number is much more reduced by lowering the temperature by 20 K; I-structures are stable for most of the displacements and only 49.9 (3.9%) of total modes are unstable. A further decrease by 20 K reduces the number only slightly, 40.1 modes (3.1%). Again, a large difference in the number of imaginary modes between 233 and 213 K is observed. We also performed the same analysis for cubic ice at 213 K. In ice, there are some imaginary modes, 37.3 out of total 1293 modes (2.9%), which are unstable in only local space and do not have the crystalline structure collapsed during the simulation run.

E. Potential energy surface and the fragile–strong transition

The potential energy surface of a fragile liquid involves numerous multilevel potential energy wells and what kind of potential energy wells the trajectory can cover depends seriously on the temperature. On the other hand, a strong liquid has Arrhenius type temperature dependence of the viscosity; the logarithm of shear viscosity versus inverse of temperature (Angell plot) is a straight line, which indicates that there is a single excitation process, suggesting a rather regular potential surface.[42] As shown in Fig. 1, the potential energy in Q-structure significantly decreases with decreasing the temperature in the range from 298 to 233 K. This leads us to a conclusion that water in this temperature range is a fragile liquid in the strong–fragile classification. A measurement of viscosity supports this view.[29] The fact that the potential en-

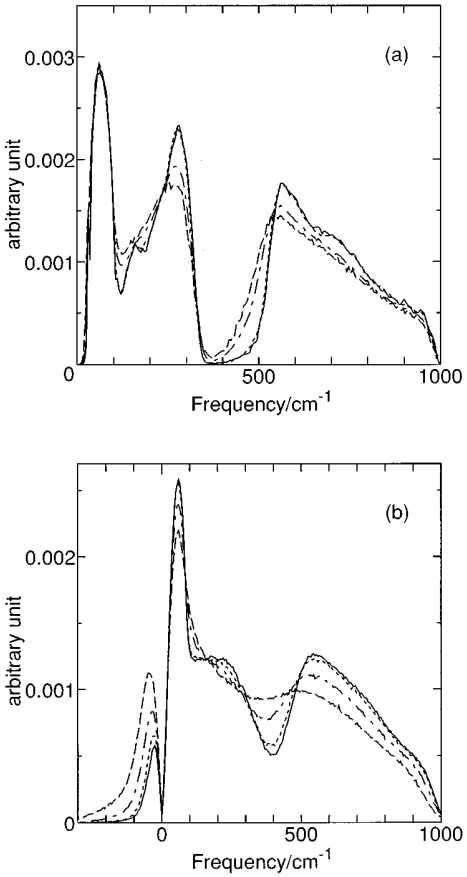

FIG. 9. Densities of state for intermolecular vibrational motions at 298, 233, 213, and 193 K and at 0.1 MPa. (a) Quenched structures, 193 K (solid line), 213 K (dotted line), 233 K (dash–dot line), 298 K (dashed line). (b) Instantaneous structures, 193 K (solid line), 213 K (dotted line), 233 K (dash–dot line), 298 K (dashed line). Imaginary modes are shown in negative frequency region. The ordinate axis unit is arbitrary.

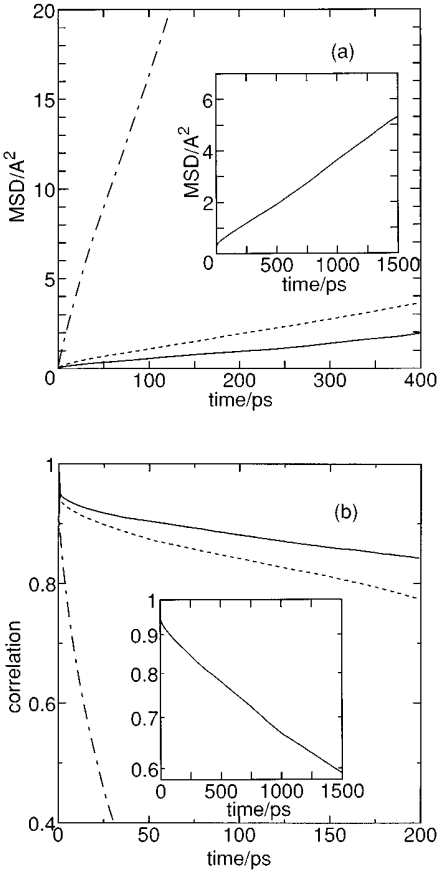

FIG. 10. (a) Mean square displacement for water at 193 K (solid line), 213 K (dotted line) and 233 K (dash–dot line) at pressure 0.1 MPa. (b) Dipole autocorrelation functions for water at 193 K (solid line), 213 K (dotted line) and 233 K (dash–dot line). The long time behaviors at 193 K are given in the insets.

ergy in Q-structure is insensitive to the temperature change implies that water blow 213 K (in TIP4P model) is a strong liquid.

A simple extrapolation of the potential energy for Q-structure above 233 K intersects with the energy of cubic ice in its Q-structure at around 160 K. Unless there is a break in the potential energy plot versus temperature between 233 and 160 K and the potential energy becomes less sensitive to temperature, the potential energy of liquid state becomes lower than that of ice. In order to preclude this Kauzmann's paradox,[10,43] water must undergo a kind of transition and the potential in Q-structure should be almost constant (against temperature) before vitrified as pointed out by Angell.[29] The transition observed around 213 K is not a glass transition since molecules even at 193 K still move more than intermolecular distances during our simulation run and the mean square displacements shown in Fig. 10(a) are linear in time, which ensures the diffusion is normal. The self-diffusion coefficients calculated from the slope of the mean square displacements are 2×10^{-6}, 9×10^{-8}, and 6×10^{-8} $\mathrm{cm^2\,s^{-1}}$ at temperature 233, 213, and 193 K, respectively. The dipole autocorrelations in Fig. 10(b) also show that reorientational motions are not frozen even at 193 K. At this temperature, most of the molecules in the whole system belong to the firmly hydrogen bonded species. As was pointed out previously,[44] firmly hydrogen-bonded molecules have smaller mobility. However, water molecules at 193 K on the average are not trapped in a local potential minimum. This means that water at 193 K is liquid phase as termed water II.

It should be addressed whether the phase behaviors at atmospheric pressure proposed here are plausible in terms of the entropy difference $\Delta S(T_1)$ between ice and LDA. Speedy[26] pointed out a large discrepancy between estimated $\Delta S(T_1)(=6\sim9\ \mathrm{J\,K^{-1}\,mol^{-1}})$ on the basis of random network model[45] (RNM) and $\Delta S(T_1)$ $(<2.9\ \mathrm{J\,K^{-1}\,mol^{-1}})$ from thermodynamic requirement that LDA and HDA free energy lines touch at T_0 (i.e., phase transition occurs). However, application of RNM does not lead to the divergent thermodynamic properties at 228 K[25] and estimation of the configurational entropy of LDA from RNM may not be justified where it is assumed there is a continuous path from normal water to LDA. In our picture, LDA is a different phase having lower entropy although LDA has a random network structure. (The difference between LDA and normal water is most conveniently viewed by hydrogen bond number distri-

butions as shown later.) Then, $\Delta S(T_1)$ can be smaller than that calculated based on RNM. Therefore, our phase diagram may not suffer from any apparent thermodynamic inconsistency and the first order transition between T_s and T_2 is plausible.

In order to check the self-consistency of our phase diagram in more detail, we evaluate the free energy components of water in LDA and HDA. The free energy A of the system is written as

$$A = U + F - k_B T \ln \Gamma, \tag{2}$$

where the mean potential energy of Q-structure and the mean free energy of intermolecular vibrations are denoted by U and F, respectively, and Γ stands for the number of Q-structures, which increases as $\exp(\sigma N)$ with respect to the number of molecules, N. Here, k_B is the Boltzmann constant. For a certain large system, such quantities as A, U, F, and $\ln \Gamma$ are all extensive properties proportional to N. Equation (2) is expressed in the form per molecule basis, thereby eliminating system size dependence as

$$a = u + f - k_B T \sigma, \tag{3}$$

where a, u, and f are properties per molecule of A, U, and F, respectively. The term $k_B \sigma$ is identified with the configurational entropy, s_c. The vibrational free energy is composed of the harmonic f_h and anharmonic f_a free energy contributions. Our simulation study is based on classical mechanics and the term f_h is easily calculated by

$$f_h / k_B T = \int_0^\infty g(\omega) \ln(\hbar \omega / k_B T) d\omega, \tag{4}$$

where $g(\omega)$ is an appropriately normalized density of state for intermolecular vibrational motions and $\hbar$ is Planck constant divided by 2π. It is difficult to calculated a reliable free energy arising from the anharmonic vibrations. This term may amount to a few kJ mol^{-1}. However, the difference between LDA and HDA is expected to be small. The logarithm of the number of configurations, $k_B \ln \Gamma / N = s_c$, configurational entropy, is dependent on the temperature in case of fragile liquid. This value changes with the phase transition. No simple way to calculate reliable s_c is known. However, it should be noted s_c^h (for HDA) is larger than s_c^l (for LDA), the latter of which may be considered to be independent of temperature if the HDA–LDA transition is accompanied by fragile–strong transition.

If the phase diagram in Fig. 5 is correct, the free energy of LDA must be equal to that of HDA at T_0. The transition temperature T_0 is tentatively set to 213 K. There is another equilibrium where ice and water exists simultaneously. Neglecting an insignificant pV term at atmospheric pressure, we can write down two equilibrium conditions as

$$u^i + f_h^i + f_a^i - T_m s_c^i = u^h + f_h^h + f_a^h - T_m s_c^h \tag{5}$$

and

$$u^l + f_h^l + f_a^l - T_0 s_c^l = u^h + f_h^h + f_a^h - T_0 s_c^h, \tag{6}$$

where superscripts l, h, and i stand for LDA, HDA, and ice. The signs of the unknown term f_a are all negative. In general, the anharmonic free energy of liquid state is lower than that of solid at the same temperature. Therefore, the inequality

$$f_a^i - f_a^h \geqslant 0 \tag{7}$$

must hold at all temperatures. It is reasonable to adopt a similar inequality to the relation between LDA and HDA phases as

$$f_a^l - f_a^h \geqslant 0. \tag{8}$$

Thus, it becomes possible to evaluate the upper bounds of the configurational entropy changes, $\Delta s_c = s_c^h - s_c^i$ and $\Delta s_c' = s_c^h - s_c^l$. That is,

$$\frac{(u^h - u^i + f_h^h - f_h^i)}{T_m} \geqslant \Delta s_c \tag{9}$$

and

$$\frac{(u^h - u^l + f_h^h - f_h^l)}{T_0} \geqslant \Delta s_c'. \tag{10}$$

Care must be taken for T_m value, which should be the melting point for TIP4P water, $T_m \simeq 240$ K (or a little bit higher).[46] In Fig. 11, the left-hand sides of inequalities (9) and (10) are plotted against temperature. The filled circles are corresponding equilibrium temperatures. This predicts the upper bound of the configurational entropy of melting, 7.7 J K^{-1} mol^{-1}. The entropy of the transition from HDA to LDA is approximately 6.1 J K^{-1} mol^{-1}. This value is quite large and the entropy difference between ice and LDA is very small, only 1.6 J K^{-1} mol^{-1} or less. The number of defects in LDA is much smaller than in HDA. A further detail on the origin of small entropy for LDA is not fully understood at present time but this is consistent with the condition that LDA undergoes first-order transition. How-

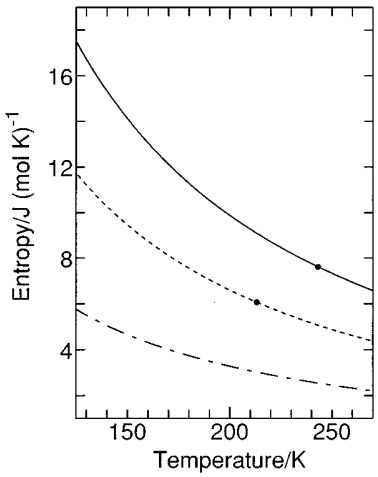

FIG. 11. Partial free energy differences divided by temperature. The partial free energy is calculated as a sum of the potential energy at quenched structure and the harmonic vibrational free energy. Solid line; free energy difference between cubic ice and HDA, dashed line; free energy difference between LDA and HDA, dash–dot line; free energy difference between LDA and ice. The dash–dot line does not correspond to the realistic entropy difference between LDA and ice at any temperature.

ever, the conjecture that LDA is a distinct phase from normal water survives. Thus, we have reconciled the idea due to Stanley *et al.*[14,37] by shifting the second critical point with Speedy's conjecture.[26]

F. Difference in hydrogen bond number distribution between pure water and aqueous solution

It is quite reasonable that the structural change in the transition is related to a difference in hydrogen bond network since it is the hydrogen bond that contrasts water to other liquid. At temperatures examined here, a probability for a pair of adjacent molecules to be hydrogen bonded is well above the percolation threshold for any reasonable criterion for the hydrogen bond and the hydrogen bonded network is spread over an entire system. A topological difference of the network pattern between two phases may be found. However, a comparison is made here simply by calculating hydrogen bond number distributions. Again, use of hydrogen bonds in Q-structure is preferable, eliminating apparent temperature dependence of hydrogen bond number. A definition of hydrogen bond, in the present study, relies solely on the potential energy for a pair of molecules; if the interaction energy is below the criterion, the pair is regarded as a hydrogen-bonded pair. The criteria we choose are ranging from -12 to -18 kJ mol^{-1}. A water molecule hydrogen bonded with j other molecules is called species-j and a probability to find species-j is given by f_j. The fractions of each species characterized by the number of hydrogen bonds with neighboring molecules are tabulated in Table I. It is evident from the table that most of water molecules belong to species-4 and f_4 increases drastically upon the transition from HDA to LDA phase, at pressures 0.1 and 200 MPa. On the other hand, increase in f_4 is rather gradual with decreasing temperature at -200 MPa where no transition is observed. The mean coordination number, which is defined by the number of molecules within 3.5 Å from the center, is listed in Table II. A clear difference is seen between LDA and HDA phases.

The fact that almost all water molecules are species-4 in LDA phase is very important to delineate why addition of a small amount of salt, alcohol, or hydrogen peroxide prevents a system from being frozen to ice.[1,47,48] Those substances interact strongly with water and take part in the hydrogen bonded network at room temperature without imposing a severe free energy penalty. Although the network prevails in the entire system to form ''gel'' in pure water at room temperature down to 233 K, there are some defects as revealed in Tables I and II. The nature of those solute molecules does not qualify for the production of three dimensional network observed in LDA. However, a number of defects in normal water allow the solutes to be dissolved by forming incomplete hydrogen bond network with surrounding water molecules: Those defects in hydrogen bond network are compatible with interstitial solute molecules in normal water (HDA). If the mixing free energy is not so unfavorable (this is the case of salt, alcohol, and hydrogen peroxide), those solutes can stay in the sea of normal water even in lower temperature down to 233 K. Yet, the number of species-4 in the solutions cannot, because of the presence of solutes, exceed the threshold value above which supercooled water undergoes a transition to LDA. In LDA phase, most of water molecules are locally tetrahedral and defects to allow the solutes to form imperfect hydrogen bond network are purged. In other words, the formation of hydrogen bond network in the same manner as LDA is no longer expected. This idea, although not connected to LDA, is not new but has been proposed by Stanley and Teixeira[10] in terms of ''patch breaking species.'' This also has something to do with ''naive water,''[7] which is regarded as water having more defects than the number allowed in LDA phase. Aqueous solutions of alcohol and hydrogen peroxide are cooled down to the glass transition temperature without being crystallized to ice since no large fluctuation associated with the spinodal-like instability is expected, which leads water to ice in laboratory experiment. These solutions are classified as a fragile liquid, which is immediately seen from the Angell plot.[29] The solute molecules break hydrogen bonds to the extent that water is prohibited to be LDA phase. This entails continuous change of viscosity down to T_g. If the above account is correct, LDA (water II) hardly dissolves these solutes.[49]

G. Coarse graining of Q-structure

A question as to how the potential energy is lowered by lowering the temperature to 233 K is addressed here. The potential surface at room temperature (298 K) seems to be complicated and transitions from one minimum (Q-structure) to another take place frequently. As has been shown in our previous study,[2,28] a set of local minimum structures are close together in configuration space. The distances between successive structures in configuration space are generally small but infrequent jump-like transitions result in large distance movements. This suggests that those structures may constitute a group. The infrequent but large-distance jump discriminates one group from another. The representative structure of this group is obtained by the coarse graining of a series of quenched structures in a similar way as was made in realization of V-structure.[50,51] The coarse graining consists of two steps;[52] the averaging the successive Q-structures over 2 ps and the subsequent quenching. The average process is performed according to

$$\overline{\mathbf{R}}_i(t)=\frac{1}{\Delta\tau}\int_{-\Delta\tau/2}^{\Delta\tau/2}\mathbf{R}_i(t+\tau)d\tau, \tag{11}$$

where $\mathbf{R}_i(t)$ is the coordinate (both translational and orientational) of ith molecule at time t and $\overline{\mathbf{R}}_i(t)$ is the averaged coordinate over $\Delta\tau(=2$ ps). In our MD simulation, the volume may fluctuate. The size of the basic cell is scaled to the mean value for the coarse graining.

The coarse graining is repeated for $(n=)30$ times. The potential energies for those structures are given in Table III. The potential energies for Q- and coarse-grained structures are plotted in Fig. 12. The potential energy after coarse graining is almost always lower than the simply quenched structures (i.e., $n=0$). This implies that the coarse-graining procedure eliminates higher potential energy structures from

TABLE I. Hydrogen bond number per molecule. Hydrogen bond energies ν are ranging from -12 to -18 kJ mol^{-1}.

	1	2	3	4	5
$p=0.1$					
T	$\nu=$	-12			
233	0	0.005	0.101	0.838	0.055
213	0.0	0.001	0.040	0.939	0.020
193	0.0	0.001	0.041	0.934	0.023
T	$\nu=$	-14			
233	0	0.014	0.144	0.802	0.039
213	0.0	0.003	0.060	0.922	0.015
193	0.0	0.004	0.070	0.910	0.016
T	$\nu=$	-16			
233	0.003	0.045	0.251	0.680	0.021
213	0.001	0.016	0.161	0.814	0.008
193	0.001	0.019	0.171	0.799	0.101
T	$\nu=$	-18			
233	0.020	0.140	0.400	0.432	0.007
213	0.008	0.081	0.359	0.549	0.002
193	0.011	0.081	0.335	0.570	0.003
$p=200$					
T	$\nu=$	-12			
233	0.0	0.006	0.127	0.796	0.071
213	0.0	0.005	0.113	0.817	0.066
193	0.0	0.003	0.085	0.865	0.048
173	0.0	0.001	0.044	0.920	0.035
T	$\nu=$	-14			
233	0.001	0.018	0.192	0.741	0.048
213	0.0	0.015	0.175	0.766	0.044
193	0.000	0.010	0.151	0.806	0.033
173	0.000	0.004	0.090	0.883	0.023
T	$\nu=$	-16			
233	0.004	0.060	0.311	0.600	0.025
213	0.003	0.053	0.299	0.622	0.023
193	0.002	0.043	0.282	0.654	0.018
173	0.0	0.019	0.208	0.759	0.014
T	$\nu=$	-18			
233	0.028	0.181	0.429	0.352	0.008
213	0.025	0.175	0.425	0.367	0.007
193	0.019	0.158	0.426	0.389	0.007
173	0.009	0.119	0.403	0.464	0.004
$p=-200$					
T	$\nu=$	-12			
233	0.0	0.003	0.076	0.891	0.030
213	0.0	0.001	0.049	0.931	0.019
193	0.0	0.000	0.017	0.972	0.012
T	$\nu=$	-14			
233	0.0	0.007	0.098	0.872	0.022
213	0.0	0.003	0.066	0.918	0.013
193	0.0	0.000	0.022	0.970	0.007
T	$\nu=$	-16			
233	0.001	0.021	0.173	0.791	0.013
213	0.0	0.011	0.132	0.850	0.006
193	0.0	0.002	0.077	0.916	0.006
T	$\nu=$	-18			
233	0.009	0.087	0.337	0.562	0.005
213	0.007	0.066	0.308	0.616	0.002
193	0.0	0.027	0.238	0.733	0.001

temporal equilibrium positions in the same sense that the V-structure is obtained by eliminating large distortions.[50,51] A group of quenched structures seem to have a hierarchical structure in configuration space. Each group, which is distant from another group, can be represented by the coarse-grained structure, which is similar to what we called ''overall inherent structures'' in the previous study.[3,35,53] The same procedures are made for lower temperature systems, 233 and 193

TABLE II. Mean coordination number for water. The coordination number is defined as the number of water molecules within 3.5 Å from the central molecule.

T	253	233	213	193	173
$p=0.1$	4.69	4.55	4.19	4.28	
$p=200$		5.23	5.24	5.09	4.32
$p=-200$	4.19	4.12	4.11	4.05	

K; $\Delta\tau/2$ is taken as 50 ps. However, the potential energies of the coarse-grained structures at 233 and 193 K do not decrease unlike the higher temperature case.

The simplest way to examine the tetrahedral coordination of each water molecule is to evaluate the contributions of the potential energy separately; a term arising from the coulombic interaction and a term from the Lennard-Jones part. The former can be a measure of tetrahedrality. If the latter term contributes significantly, the structure is that of the simple liquid. Those two terms for water systems are also listed in Table III. As the total energy becomes lower, the Lennard-Jones part increases and the tetrahedral coordination is enhanced sacrificing the oxygen–oxygen repulsive interaction.

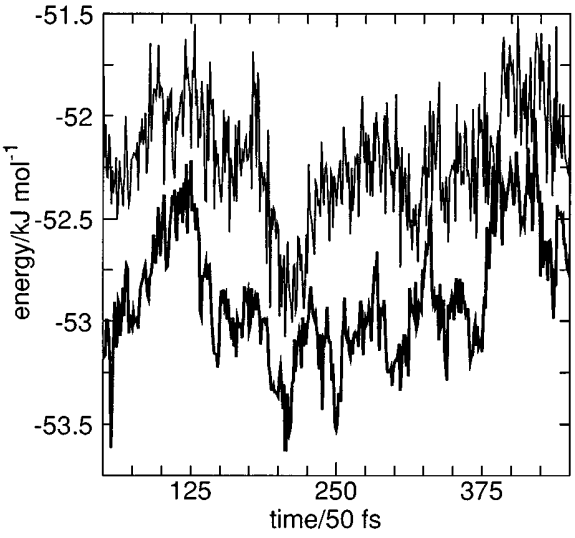

FIG. 12. Time evolution of the potential energies for quenched structure (upper, solid line) and coarse-grained structure (lower, heavy solid line) at 298 K for 20 ps. Coarse-graining cycles are repeated for 30 times. The first and the last 50 data are not shown since an edge effect is large in calculating coarse-grained structures.

IV. CONCLUDING REMARKS

The anomalies of supercooled water in thermodynamic response functions at atmospheric pressure, the phase transition between LDA and HDA and the predicted fragile–strong transition are accounted for in a unified manner by reconciling two conjectures so far proposed; (1) a second critical point separating LDA and HDA ices due to Stanley and co-workers, (2) existence of a different phase from a normal water, called water II proposed by Speedy. A new phase diagram for supercooled water is proposed on the basis of extensive MD simulations. At atmospheric pressure, thermodynamic properties, structures, and dynamic properties of TIP4P water have discontinuities around 213 K suggesting liquid–liquid phase transition, which is an extension of the LDA–HDA transition experimentally observed at high pressure. In the new phase diagram, the locus of the second critical point is moved into negative pressure region. Thus, it becomes possible to account for the divergence of the thermodynamic response functions at atmospheric pressure in terms of the large critical fluctuation and/or the spinodal-like instability of HDA. The unstable HDA undergoes a transition to LDA phase. It is difficult from this limited size of simulation to identify whether the transition is first order. However, our observation, the discontinuities in thermodynamic properties in high pressure region such as +200 MPa and continuous changes at negative pressure −200 MPa, encourages an idea of the first-order phase transition. Our simulation results at −200 MPa also show RDF and the density of state exhibit much smaller temperature dependence than those at atmospheric pressure. This reinforces our proposed phase diagram and gives rationale to the existence of the second critical point between 0 and −200 MPa. It is also discussed that the HDA–LDA transition entails a fragile-strong transition.

TABLE III. Total and Lennard-Jones (LJ) part of potential energy (in kJ mol^{-1}) at 0.1 MPa and various temperatures and those for coarse-grained structure after n cycles at 0.1 MPa and 298 K.

n	Total	LJ
0	−52.20	10.69
5	−52.56	11.27
10	−52.70	11.54
15	−52.77	11.63
20	−52.80	11.70
25	−52.84	11.80
30	−52.89	11.84
T	Total	LJ
298	−52.18	10.64
273	−52.44	10.80
253	−52.85	10.88
233	−53.37	11.19
213	−54.97	12.26
193	−55.07	12.32

Since two different amorphous phases at high pressure are known experimentally,[4] the phase boundary separating LDA and HDA must go down to a certain pressure on the temperature–pressure plane. Moreover, that T_s, the temperature of the stability limit decreases with increasing pressure[54] is in good correspondence to the negative slope of (dp/dT) along the coexistence curve since the volume and entropy changes have different signs. Two disordered phases may have a critical point. Then, we are left with only two possible ways as to the phase behaviors at atmospheric pressure. The phase boundary may be terminated either in positive pressure or in negative pressure. The former is the picture drawn by Poole *et al.*[14] where supercooled water has a

continuous path to LDA. The latter is the scenario proposed here; the coexistence line enters into negative pressure region and water at atmospheric pressure necessarily undergoes a transition, which is the same as observed at high pressure. In practice, the transition may occur not at the intersect with coexistence line but at the intersect with the spinodal line. An idea underlying the proposed phase diagram is the first order phase transition between two liquid phases, though it is not explicitly demonstrated from MD simulations because of the limited system size. All the properties shown do not contradict with our conclusion that the LDA–HDA transition is similar to that of gas–liquid. The density difference can be an order parameter as is the case of gas–liquid equilibrium.

ACKNOWLEDGMENTS

The author thanks Professors, I. Ohmine, M. Sasai, and H.E. Stanley and Dr. R. Yamamoto and Dr. K. Koga for helpful discussion and I. Okabe for providing cubic ice structures. This work is supported by Grant-in-Aid from the Ministry of Education, Science and Culture and also by the Computer Center of Institute for Molecular Science.

[1] C. A. Angell, in *Water: A Comprehensive Treatise*, edited by F. Franks (Plenum, New York, 1981), Vol. 7, Chap. 1; Annu. Rev. Phys. Chem. **34**, 539 (1983).
[2] I. Ohmine and M. Sasai, Prog. Theor. Phys. Suppl. **103**, 61 (1991).
[3] I. Ohmine and H. Tanaka, Chem. Rev. **93**, 2545 (1993).
[4] O. Mishima, L. D. Colvert, and E. Whalley, Nature **310**, 393 (1984); **314**, 76 (1985).
[5] D. Eisenberg and W. Kauzmann, *The Structure and Properties of Water* (Oxford University Press, London, 1969).
[6] O. Mishima, J. Chem. Phys. **100**, 5910 (1994).
[7] R. J. Speedy and C. A. Angell, J. Chem. Phys. **65**, 851 (1976).
[8] C. A. Angell, M. Oguni, and W. J. Sichina, J. Phys. Chem. **86**, 998 (1982).
[9] R. J. Speedy, J. Phys. Chem. **86**, 982 (1982).
[10] H. E. Stanley and J. Teixeira, J. Chem. Phys. **73**, 3404 (1980).
[11] M. Sasai, J. Chem. Phys. **93**, 7329 (1990).
[12] S. Sastry, F. Sciortino, H. E. Stanley, J. Chem. Phys. **98**, 9863 (1993).
[13] P. G. Debenedetti and M. C. D'Antonio, J. Chem. Phys. **84**, 3339 (1986); M. C. D'Antonio and P. G. Debenedetti, *ibid.* **86**, 2229 (1987).
[14] P. H. Poole, F. Sciortino, U. Essmann, and H. E. Stanley, Nature **360**, 324 (1992); Phys. Rev. E **48**, 3799 (1993).
[15] G. P. Johari, A. Hallbrucker, and E. Mayer, Nature **330**, 552 (1987).
[16] A. Hallbrucker, E. Mayer, and G. P. Johari, Philos. Mag. B **60**, 179 (1987).
[17] D. D. Klug and Y. P. Handa, J. Phys. Chem. **92**, 3323 (1988).
[18] G. P. Johari, G. Astl, and E. Mayer, J. Chem. Phys. **92**, 809 (1990).
[19] M. Sugisaki, H. Suga, and S. Seki, Bull. Chem. Soc. Jpn. **41**, 2591 (1968).
[20] G. P. Johari, Philos. Mag. **35**, 1077 (1977).
[21] C. A. Angell and J. C. Tucker, J. Phys. Chem. **84**, 268 (1980).
[22] A. Hallbrucker and E. Mayer, J. Phys. Chem. **91**, 503 (1987).
[23] D. R. Macfarlane and C. A. Angell, J. Phys. Chem. **88**, 759 (1984).
[24] S. A. Rice, M. Bergren, and L. Swingle, Chem. Phys. Lett. **59**, 14 (1978).
[25] M. G. Sceats and S. A. Rice, in *Water: A Comprehensive Treatise*, edited by F. Franks (Plenum, New York, 1981), Vol. 7, Chap. 2.
[26] R. J. Speedy, J. Phys. Chem. **96**, 2322 (1992).
[27] P. H. Poole, F. Sciortino, F., T. Grande, H. E. Stanley, and C. A. Angell, Phys. Rev. Lett. **73**, 1632 (1994).
[28] H. Tanaka, Nature **380**, 328 (1996).
[29] C. A. Angell, J. Phys. Chem. **97**, 6339 (1993); in *Hydrogen Bond Networks*, edited by M-.C. Bellissent-Funel, and J. C. Dore (Kluwer, Dordrecht, 1994), pp. 3–22.
[30] S. Nosé, Mol. Phys. **52**, 255 (1984); J. Chem. Phys. **81**, 511 (1984).
[31] H. C. Andersen, J. Chem. Phys. **72**, 2384 (1980).
[32] W. L. Jorgensen, J. Chandrasekhar, J. D. Madura, R. W. Impey, and M. L. Klein, J. Chem. Phys. **79**, 926 (1983).
[33] P. H. Poole, U. Essmann, F. Sciortino, and H. E. Stanley, Phys. Rev. E **48**, 4605 (1993).
[34] F. H. Stillinger and T. A. Weber, J. Phys. Chem. **87**, 2833 (1983).
[35] I. Ohmine, H. Tanaka, and P. G. Wolynes, J. Chem. Phys. **89**, 5852 (1988).
[36] If we tentatively adopt a critical exponent of $\beta=1/3$ for $\rho_h-\rho_l=(T/Tc'-1)^{\beta}$, the critical temperature is higher by 0.3 to 0.4 K than the intersect (213 K) with atmospheric pressure line. Then, the critical pressure is not lower than -5 MPa if (dp/dT) along the coexistence line does not change from that estimated at 0.1 MPa. Even if we adopt an exponent of $\beta=0.5$ from a mean field theory, the critical pressure is not lower than -20 MPa.
[37] H. E. Stanley, C. A. Angell, U. Essmann, M. Hemmati, P. H. Poole, and F. Sciortino, Physica A **205**, 122 (1994).
[38] E. G. Ponyatovskii, V. V. Sinitsyn, and T. A. Pozdnyakova, JETP Lett. **60** 360 (1994).
[39] M-.C. Bellissent-Funel and L. Bosio, J. Chem. Phys. **102**, 3727 (1995).
[40] MD simulations for monatomic fluid interacting via Lennard-Jones potential have been performed at temperature 1.25 in LJ reduced unit which is just below its (gas–liquid) critical point, and at pressure 0.10. The critical temperature and pressure are 1.313 and 0.13, see J. K Johnson, J.A. Zollweg, and K.E. Gubbins, Mol. Phys. **78**, 591 (1993). The density fluctuates in a range from 0.01 to 0.5 and its mean values is approximately the same as the critical density 0.3.
[41] I. Ohmine and H. Tanaka, J. Chem. Phys. **93**, 8138 (1990).
[42] F. H. Stillinger, J. Chem. Phys. **88**, 7818 (1988).
[43] W. Kauzmann, Chem. Rev. **43**, 219 (1948).
[44] F. Sciortino, A. Geiger, and H. E. Stanley, Nature **354**, 218 (1991).
[45] M. G. Sceats and S. A. Rice, J. Chem. Phys. **72**, 3260 (1980).
[46] O. A. Karim and A. D. J. Haymet, J. Chem. Phys. **89**, 6889 (1988).
[47] C. A. Angell and E. J. Sare, J. Chem. Phys. **52**, 1058 (1970).
[48] M. Oguni and C. A. Angell, J. Chem. Phys. **73**, 1948 (1980).
[49] C. M. Sorensen, in *Physical Chemistry of Aqueous Systems*, edited by H. J. White, J. V. Sengers, D. B. Neumann, and J. C. Bellows (Begell House, New York, 1995), pp. 308–316.
[50] F. Hirata, P. J. Rossky, J. Chem. Phys. **74**, 6867 (1981).
[51] H. Tanaka and I. Ohmine, J. Chem. Phys. **87**, 6128 (1987).
[52] H. Tanaka, Mol. Sim. **16**, 87 (1996).
[53] This point is not clear from only those shown in the text. In a fairly large number of molecules, only 30 cycles of the coarse graining do not take effect appreciably. When we adopt a system with smaller number of water molecules such as 64, the number of Q-structures in configuration space is rather limited and the number of structures after coarse graining is much reduced: The number of independent structures, 523 obtained from simple quenching was much reduced to 113 after 50 cycles of coarse graining when the number of water molecules was 64. See Ref. 52.
[54] H. Kanno and C. A. Angell, J. Chem. Phys. **70**, 4008 (1979).